

PAPER

## Elastic–plastic properties of graphene engineered by oxygen functional groups

To cite this article: Yuan Hou *et al* 2017 *J. Phys. D: Appl. Phys.* **50** 385305

View the [article online](#) for updates and enhancements.

### Related content

- [Elastic, plastic, and fracture mechanisms in graphene materials](#)  
Collin Daniels, Andrew Horning, Anthony Phillips *et al.*
- [Mechanical properties of borophene films: a reactive molecular dynamics investigation](#)  
Minh Quy Le, Bohayra Mortazavi and Timon Rabczuk
- [The fracture toughness of graphene during the tearing process](#)  
Ying Wang and Zishun Liu



**IOP | ebooks™**

Bringing you innovative digital publishing with leading voices to create your essential collection of books in STEM research.

Start exploring the collection - download the first chapter of every title for free.

# Elastic–plastic properties of graphene engineered by oxygen functional groups

Yuan Hou<sup>1,2</sup>, YinBo Zhu<sup>1</sup> , XiaoYi Liu<sup>1</sup>, ZhaoHe Dai<sup>2</sup>, LuQi Liu<sup>2</sup>, HengAn Wu<sup>1</sup> and Zhong Zhang<sup>1,2</sup>

<sup>1</sup> CAS Key Laboratory of Mechanical Behavior and Design of Materials, Department of Modern Mechanics, CAS Center for Excellence in Nanoscience, University of Science and Technology of China, Hefei, Anhui 230027, People's Republic of China

<sup>2</sup> CAS Key Laboratory of Nanosystem and Hierarchical Fabrication, National Center for Nanoscience and Technology, Beijing, 100190, People's Republic of China

E-mail: [wuha@ustc.edu.cn](mailto:wuha@ustc.edu.cn) (HAW) and [zhong.zhang@nanoctr.cn](mailto:zhong.zhang@nanoctr.cn) (ZZ)

Received 3 May 2017, revised 4 July 2017

Accepted for publication 14 July 2017


Published 1 September 2017



## Abstract

Using molecular dynamics (MD) simulations, we investigate the elastic–plastic mechanical performances of monolayer graphene oxide (GO) under uniaxial tension. The brittle–ductile–brittle transition and nonlinear–linear–nonlinear elastic transition is found in the uniaxial tension of GO, which displays strong correlations to the content, distribution and proportion of oxygen functional groups. In principle, the tensile behavior of graphene with epoxy groups exhibits ductile fracture features due to the unique epoxy-to-ether transformation in structural evolution. Our simulation results also reveal that wrinkling could cause a competing mechanism of strain-hardening or -softening, and in turn, the nonlinear–linear elasticity transition. Moreover, we propose a continuum mechanical model with a modified stress–strain relation to understand the unique deformation performances, which is consistent with the MD results. These findings might provide valuable insight and design guidelines for optimizing the specific mechanical properties and deformation behaviors of graphene and its derivatives.

Keywords: graphene, elastic–plastic properties, MD simulation, oxygen functional group

 Supplementary material for this article is available [online](#)

(Some figures may appear in colour only in the online journal)

## Introduction

The first two-dimensional (2D) atomic crystal available, graphene—a closely packed 2D  $sp^2$ -bonded carbon honeycomb lattice—has proven to be a remarkable material because of its unique physical properties [1–5]. However, for various practical applications of graphene sheets, such as nanocomposites [6, 7], nano/micro-scale systems [8–10] and macroscopically multifunctional self-assemblies [11–13], the emergence of chemical modification in the graphene lattice is inevitable or even essential, either because of the production process or operating requirements. For instance, functionalizing graphene sheets with various oxygen functional groups is critical for the desired interfacial adhesions in graphene-based

nanocomposites, in which the outstanding mechanical performance of graphene can be effectively transferred across a multiple length scale up to the macroscopic level [14–17]. Apart from being a precursor for graphene, the surface-rich oxygen functional groups of graphene oxide (GO) provide its excellent properties, and hence GO itself can be useful in flexible electronics, battery electrodes, and paper-like composite materials [18–24].

In addition to the elegant process of GO-based multifunctional applications, GO also offers the significant opportunity to fundamentally explore how the chemical functionalities influence the atomistic mechanical performance on its basal plane. Zheng *et al* reported that Young's modulus depends greatly on the degree of functionalization [25]. Liu *et al*

comparatively studied Young's modulus and the intrinsic strength of amorphous and ordered GOs by first-principles calculations [26]. Some theoretical and experimental measurements also revealed the effective Young's modulus and intrinsic strength of GO and its dependence on the density of the oxygen functional groups [27–31]. More recently, some novel mechanical phenomena have been observed in a one-atom-thick sheet such as flaw insensitivity [32–36], chemical functionality-induced plasticity and ductility on GO [37].

Although these studies validate the fact that the variety and content of the oxygen functional groups can significantly affect the mechanical properties and behaviors of GO, the relationship between the structure and mechanical properties at the atomic scale is still not comprehensively understood, especially for the underlying mechanism of anomalous mechanical behaviors, such as the plasticity and linear elasticity of GO. Furthermore, it is of great importance to study not only the strength and stiffness but the fracture and deformation performance of graphene for its electro-mechanical applications. An interesting question, which has not been answered in previous studies, is how different functionalizations affect the mechanical behavior of GO. Actually, due to the complexity of the nanostructure of GO, more theoretical studies and simulations are needed to solve this problem.

In this study, we reveal that the content, distribution and proportion of oxygen functional groups dominate the mechanical properties of GO. Using molecular dynamics (MD) simulations, we demonstrate some anomalous in-plane mechanical properties of GO with different distributions of epoxy groups and hydroxyl groups which stem from the unique epoxy-together transformation during structural evolution. These results reveal a unique perspective to engineer the elastic–plastic properties of graphene via oxygen functional groups.

## Models and methods

The first principles-based reactive force field (ReaxFF) was used in the MD simulations to describe the mechanical and chemical behaviors as well as the bond formation and fracture of graphene and GO using the LAMMPS package [38]. The ReaxFF potential function uses distance-dependent bond-order functions to represent the contributions of chemical bonding to the potential energy. The intralayer chemical interaction such as the covalent bond and hydrogen bond are both considered, while long-range forces between different layers, such as the hydrogen bond and van der Waals interaction, are not considered [15, 38–44]. In our MD simulations, both the formation or recombination of chemical bonds are considered in the simulations at the same time because the formation or recombination of the chemical bonds could occur simultaneously. The ReaxFF parameter set used in this manuscript was provided by the supplemental information in previous work [45]. The MD simulation was performed in the NPT ensemble using the Nose–Hoover thermostat to enable volume variation, and the temperature was controlled at 300 K with a damping constant of 100 fs [46]. The pressure of the system was kept at 0 atm during thermal equilibration to eliminate the influence of

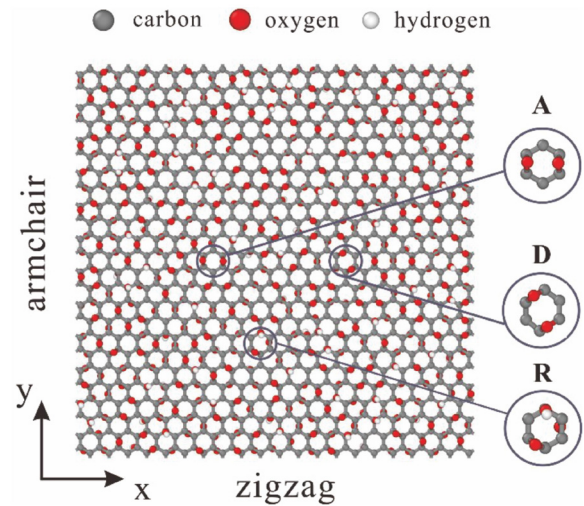


**Figure 1.** Top view of the monolayer graphene oxide (GO) with randomly distributed oxygen functional groups in the MD simulations, where A and D represent the armchair-arranged and diagonally-arranged epoxy groups, respectively, and R represents the randomly-arranged epoxy and hydroxyl groups. The gray balls denote carbon atoms in GO. The red and white balls represent oxygen and hydrogen atoms, respectively.

external pressure on the material properties. After the structure was relaxed for 10 ps, the uniaxial strain-controlled tension was applied by deforming the simulation box along the  $x$  or  $y$  direction (zigzag or armchair, as can be seen in figure 1). The time history of the pressure and temperature for the late period of the 10 ps equilibration of these samples is shown in figure S1 (available online at [stacks.iop.org/JPhysD/50/385305/mmedia](https://stacks.iop.org/JPhysD/50/385305/mmedia)) to verify the stability of the GO model. In our simulations, a time step of 0.25 fs was used in the velocity-Verlet integrator. Periodic boundary conditions were imposed in all three directions. The 2 nm vacuum layers were maintained along the  $z$  direction to ensure the free surface of monolayer GO. Energy minimization was performed using a conjugate-gradient algorithm with an energy-convergence criterion. The virial stress tensor was computed with the assumed thickness (0.7 nm) of monolayer GO [47]. The equivalence of the virial stress and Cauchy stress has been verified [48]. Based on the theory of continuum mechanics, the Cauchy stresses are related to the second Piola–Kirchhoff stresses  $\Sigma$  as [49]:

$$\Sigma = JF^{-1}\sigma(F^{-1})^T, \quad (1)$$

where  $J$  is the determinant of the deformation gradient tensor  $F$ .

The Lagrangian strain  $\eta$  is determined by the engineering strain  $\varepsilon$  via the equation [49]:

$$\eta = \varepsilon + \frac{1}{2}\varepsilon^2. \quad (2)$$

In fact, the atomistic structure of monolayer GO is complicated and remains controversial. Many experiments demonstrated that GO contains several typical oxygen functional groups such as epoxy, hydroxyl, carbonyl, carboxyl, etc [50–52], but epoxy and hydroxyl groups have been studied mostly for their impact on mechanical properties [26, 27, 53].

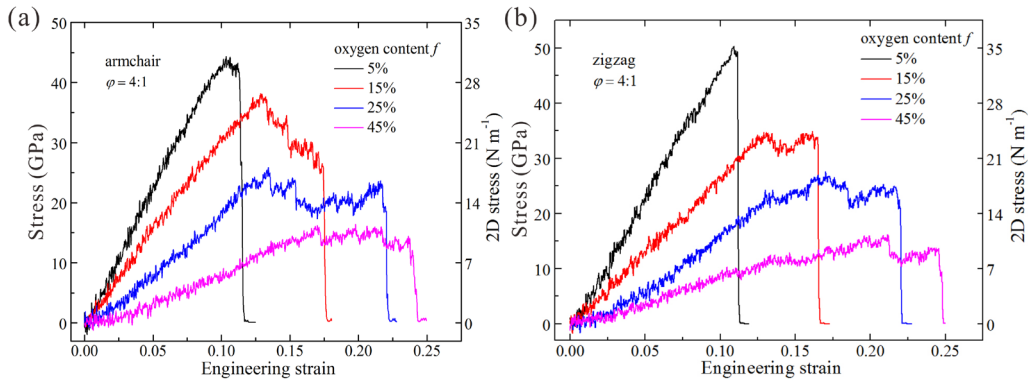


**Figure 2.** (a), (b) Mechanical properties (stress–strain) of monolayer GO ( $f = 0.15$ ,  $\varphi = 4$ ) under uniaxial tension in the armchair and zigzag direction, respectively.

Even though the experiments demonstrated that GO is amorphous [54, 55], some theoretical investigations suggested that the ordered structures are thermodynamically favorable [56–58]. Three basic hexagonal units in the GO model are illustrated in figure 1, marked as A (epoxy groups arranged in the armchair direction), D (epoxy groups arranged in the diagonal direction), and R (epoxy and hydroxyl groups randomly arranged), respectively. To investigate the mechanical properties of GO and the corresponding mechanisms, MD models were built based on the three different atomistic distributions of oxygen functional groups in figure 1, that is, A-GO, D-GO, and R-GO, respectively. Here, the oxygen content is defined as  $f = N_{\text{oxygen}}/N_{\text{carbon}}$ , and the ratio among different functional groups is defined as  $\varphi = N_{\text{epoxy}}/N_{\text{hydroxyl}}$ . For example, as shown in figure 1, a  $5.0 \times 5.0 \text{ nm}^2$  GO monolayer model consisting of 1008 carbon atoms was constructed with 280 epoxy groups and 70 hydroxyl groups randomly positioned ( $f = 0.35$ ,  $\varphi = 4$ ).

## Results and discussion

### The influence of the content of oxygen functional groups

Previous experimental studies revealed that the oxygen content of GO is variable which has a great influence on the physical properties of GO (the studies revealed that varying the content of oxygen in GO influences the physical properties of GO) [59, 60]. Engineering the mechanical properties of GO by means of (modulating/changing) the oxygen content is an effective method for researchers. According to previous studies, a series of uniaxial tensile MD simulations were performed over a wide range of the oxygen content ( $0.05 \leq f \leq 0.45$ ) in order to study the influence of oxygen content on the mechanical properties of GO ( $\varphi = 4:1$ ). Interestingly, when the oxygen content  $f$  increases, the monolayer GO turns into plastic and then transforms from ductile fracture into brittle fracture since the oxygen content reaches the critical value, as shown in figures 2(a) and (b). This means that there is a brittle–plastic–brittle transition in amorphous GO with an increase in oxygen content. For GO with low oxygen content ( $f \leq 0.05$ ), the fracture mode is the same as that of pure graphene, which is brittle because of the linear defect evolution [61]. When the oxygen

content increases ( $f = 0.05–0.25$ ), the closed-ring defect evolution induced by the epoxy-to-ether transformation causes a ductile fracture, which has been verified in experiments [37]. When the content of the oxygen functional groups is larger than a certain proportion ( $f \geq 0.45$ ), the  $sp^3$  C–O–C bond network will be the main load-bearing part instead of the mixed network of  $sp^2$  and  $sp^3$  C–C bonds, resulting in linear crack propagation because of the absence of an energy difference. Compared with the results in armchair and zigzag tension, it can be found that GO shows different fracture behaviors depending on the tension direction and oxygen content. The results of the strength and elastic modulus are demonstrated in figure S2. It is found that the strength in the armchair direction decreases from 100 GPa–20 GPa when the  $f$  increases from 0–0.45, while in the zigzag direction the strength reduces from 120 GPa–20 GPa. The chirality dependence of the mechanical properties of GO disappears with the increasing oxygen content, similar to the previous MD study [27]. Figure S1 shows that GO with a high oxygen content is orthogonal isotropic when the oxygen content  $f$  is larger than 0.6, which is mainly due to the role of diagonal symmetric defects, while the inset shows that the elastic modulus drops alternately, which may be attributed to the synergistic effects of the different distributions of the functional groups in amorphous GO models. Moreover, we conclude that the distributions of type A and type D will convert to each other with the increasing tensile strain as well as the oxygen content because of the large deformation of bond angles and the epoxy-to-ether transformation.

### The influence of the distribution of oxygen functional groups

To clarify the plastic property of GO, 150 epoxy groups were first distributed along the armchair direction on the monolayer A-GO ( $f = 0.15$ ,  $\varphi = \infty$ ). The oxygen atom in the epoxy group and two carbon atoms in the hexatomic ring form a triangle, as shown in figure 3(a) with a green dotted box. To obtain the tensile behavior of A-GO, uniaxial tension tests were performed in the MD simulation. Chirality-dependence exists due to the unidirectional distribution of epoxy groups, which leads to obviously different properties in the mechanics along the zigzag and armchair direction respectively. It is found that



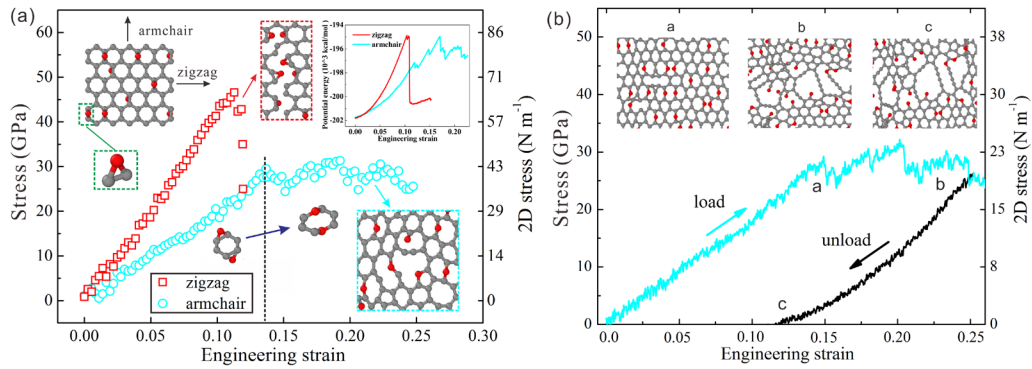


**Figure 3.** (a) Mechanical properties (stress–strain) of monolayer A-GO ( $f = 0.15$ ,  $\varphi = \infty$ ) under uniaxial tension in zigzag (red squares) and armchair (cyan circles) directions. Typical snapshots of structural evolution are exhibited in the red and cyan dotted boxes, corresponding to different defect evolution mechanisms. (b) The loading–unloading process of A-GO in the armchair direction. The insets denote snapshots in the structural evolution, corresponding to the marked locations in the stress–strain curves, respectively.

the Young's modulus is 400 GPa and the strength is 46 GPa in zigzag tension for graphene sheets with armchair-arranged epoxy groups, which is approximately twice that of armchair tension. However, the fracture strain is 0.11 in zigzag tension, which is much smaller than that in armchair tension (0.25), indicating that there are different fracture mechanisms. The fracture behaviors in the two directions further highlight such chirality-dependent mechanical performances as exhibited in the stress–strain curves (figure 3(a)). Analogous to the tearing fracture mode in pristine graphene [62], brittle fracture happens when the tensile strain is beyond 0.11 (red squares) in zigzag tension. In contrast, when the tensile test is applied in the armchair direction (cyan circles), the monolayer A-GO exhibits ductile fracture when the tensile strain is beyond 0.14. After the armchair-direction unloading of A-GO (figure 3(b)), the residual strain can be observed, demonstrating the plasticity of A-GO in armchair tension.

To shed light on the chirality-dependent plasticity, we further investigate the structural evolution of A-GO under uniaxial tension. In our simulations, the structural snapshots reveal that linear crack propagation (red dotted box in figure 3(a)) arises in zigzag tension, while closed C–O rings (cyan dotted box in figure 3(a)) form in armchair tension. Here, the armchair-arranged epoxy groups lead to this difference in the fracture behaviors. When the tensile test is applied in the armchair direction, the C–O–C triangles become the main stress structures, where the C–C  $sp^3$  bond breaks antecedent to the C–O  $sp^3$  bond, accompanied by the transformation from epoxy to ether [37]. Many hexagon units in A-GO are transformed into heptagon or octagon defects, corresponding to the dissipation of potential energy. Simultaneously, the epoxy-to-ether transformation induces the formation of polygonal closed C–O rings to suppress the crack propagation, resulting in the ductile fracture behavior for the whole structure. Consequently, the A-GO exhibits a plastic characteristic in the armchair direction. The residual strain and snapshots of the structural evolution further indicate that the closed-ring defects are irreversible and stable (figure 3(b)). Nevertheless, those armchair-arranged epoxy groups have no obvious influence on the mechanical properties of graphene oxide in zigzag tension, so linear crack propagation occurs in zigzag direction. It is

worth noting that A-GO has higher strength but with a lower fracture strain in the zigzag-direction tension test, which contrasts with the results tested in the armchair direction. Briefly, the plasticity as well as the chirality-dependent mechanical properties of GO can be achieved by armchair-directionally arranging the epoxy groups because of the closed-ring defect evolution mechanisms, which is the main reason for the ductile fracture of GO.

A different type of epoxy distribution model, D-GO ( $f = 0.15$ ,  $\varphi = \infty$ ), with 150 epoxy groups distributed along the diagonal direction, is also studied here. The stress–strain results under uniaxial tension are illustrated in figure 4(a), where the D-GO exhibits orthogonal isotropic mechanical behaviors. According to the results in figure 4(a), the strengths ( $\sigma_{s1}$ ,  $\sigma_{s2} \sim 40$  GPa) in two orthogonal directions have a close value instead of the mechanical chirality-dependency in A-GO, and Young's modulus ( $E_0 \sim 200$  GPa), calculated by fitting the initial linear part of the stress–strain curve, is also nearly identical. The schematic illustration in figure 4(b) clearly reveals the underlying mechanism of the weakening chirality-dependence observed in the D-GO samples. It can be found that the hexagon unit tends to be transformed into an octagon defect, which is typical in the diagonal symmetry. Meanwhile, the ultimate stress of D-GO is mainly determined by those defects instead of the  $sp^2$  C–C bond network since the number of epoxy groups reaches a certain proportion, resulting in orthogonal isotropic properties, as observed in the monolayer D-GO.

However, after a certain applied strain (i.e. beyond 0.04), the graphene with diagonally-arranged epoxy groups exhibits an obvious nonlinear stress–strain relation and different stiffnesses in the armchair and zigzag (directional) tension ( $E_1 \sim 310$  GPa,  $E_2 \sim 210$  GPa). Here, we propose two deformation mechanisms for this nonlinear behavior of D-GO. The first mechanism is the elongation of the C–C  $sp^2$  bonds, while the second is the elongation and rotation of the C–O  $sp^3$  bonds. Previous studies have verified that the existence of vacancy defects and the flexibility of  $sp^3$  C–C bonds can result in a significantly decreased modulus of the GO compared to that of pristine graphene [4, 30]. Similarly, the  $sp^3$  C–O bond deformation mechanism can cause a lower D-GO modulus. In our simulations, we attribute the

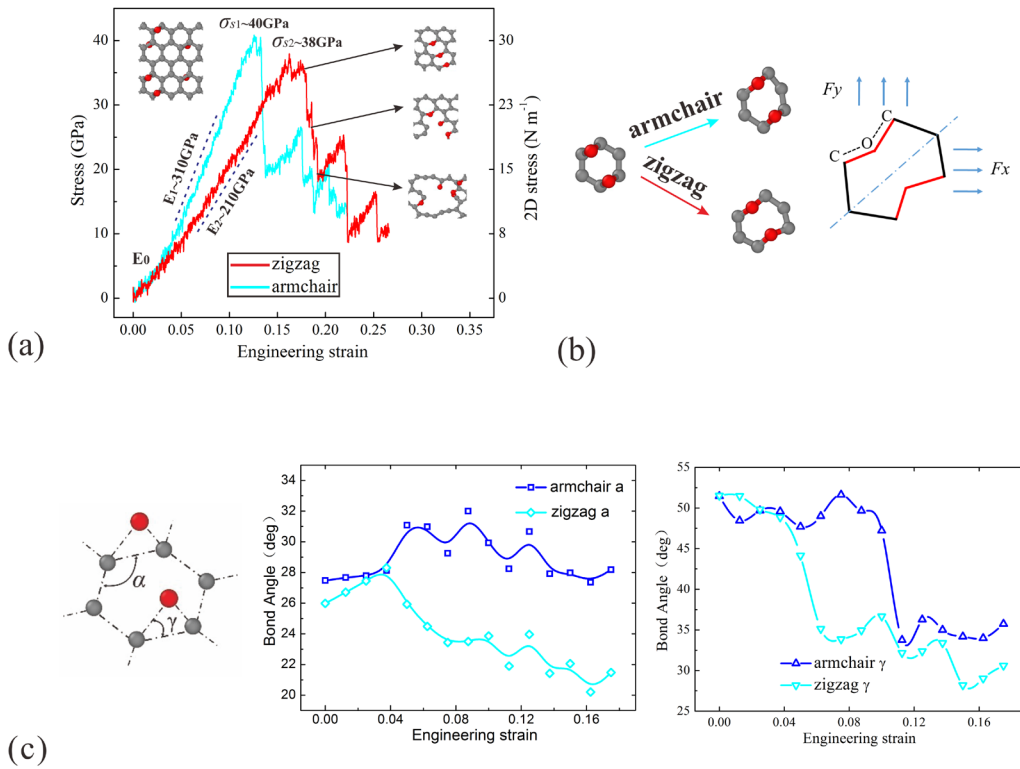


**Figure 4.** (a) Mechanical properties of monolayer D-GO ( $f = 0.15$ ,  $\varphi = \infty$ ) under uniaxial tension along the armchair (cyan) and zigzag (red) directions. (b) Schematic of the tensile deformation of a hexagonal unit. (c) The schematic of bond angles and the curves of the variation of angle  $\alpha$  and  $\gamma$ .

activation of such deformation mechanisms to the difference in the critical strains of the epoxy-to-ether transformation in two directions. This difference can be easily demonstrated by the variation of bond angles, as shown in figure 4(c), where the relevant bond angles are marked as  $\alpha$  and  $\gamma$ , respectively. Critically, when the strain is beyond 0.04,  $\alpha$  decreases gradually, which means the ether group turns to the tensile direction. Such a difference results in an easy epoxy-to-ether transformation in the zigzag-direction tension. Similarly, the bond angle  $\gamma$  shows a slump when the strain is  $\sim 0.04$  (figure 4(d)) in the armchair direction. However, in the zigzag direction,  $\gamma$  shows a slump when the strain is  $\sim 0.1$ , corresponding to the fracture strain. It should be noted that the slump of  $\gamma$  means a rise in the epoxy-to-ether transformation, resulting in the C–O  $sp^3$  bonds dominating the stiffness. In a word, diagonally-arranged epoxy groups lead to a delay in the epoxy-to-ether transformation so that the D-GO sheet shows a modulus difference under large deformation in two directional tensions.

In an effort to study the corresponding fracture behaviors, the structural snapshots of the D-GO under zigzag-direction tension are shown in the insets of figure 4(a). The stairs in the stress–strain curves indicate that a stepwise brittle fracture occurs with a decrease in the associated strength in both the armchair and zigzag directions because the stress reaches its ultimate value. In simple terms, cracks grow out from the epoxy-to-ether transformation and then propagate along the nearby C–O–C bonds, just like the longitudinal unzipping in a carbon nanotube [63]. Subsequently, metastable defects form when the strain reaches a critical value, resulting in the recovery of the tensile resistant capacity.

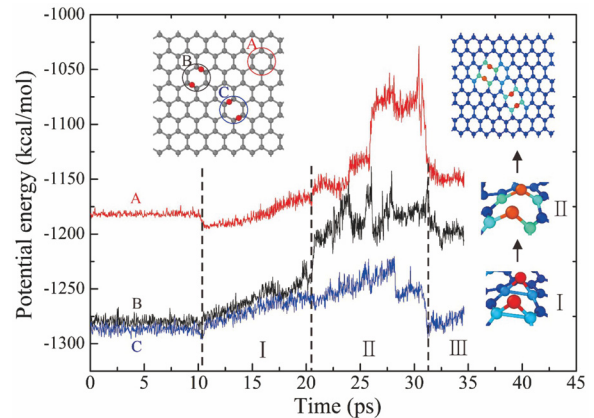


**Figure 5.** Computed potential energy of D-GO for the local distortion. Three units are marked in the upper-left inset as A, B, and C, respectively. The gray and red balls denote carbon and oxygen atoms, respectively. The red, black, and blue energy–time curves correspond to the three marked units.

Furthermore, to illustrate the local distortion during the armchair-direction tension, the potential energy curves are shown in figure 5. It is found that the epoxy-to-ether transformation causes initial destabilization in the potential energy of the structure, but the energy disturbance is limited in the local area, which verifies the metastability of such defects in D-GO. This phenomenon, described as the plasticity-like behaviors in both directional tensions, further confirms that the diagonally-arranged epoxy groups weaken the chirality-dependent plasticity of D-GO. Compared with the results of A-O, it can be concluded that the brittle–ductile–brittle transition of GO is

mainly due to the different defect evolution which is also associated with the distribution of epoxy groups. After the energy minimization in the initial stage, uniaxial tension is applied on the monolayer D-GO in the armchair direction with a constant engineering strain rate of  $10^9 \text{ s}^{-1}$ . In stage I, the potential energy curves of the three units increase linearly because of the bond stretching. The sudden enhancements in those three curves refer to the local distortions induced by chemical-bond rupture. It was found that the B-unit first distorts in the simulation, which is due to the epoxy-to-ether transformation. Then in stage II, the energy disturbance is limited within the local area so that the whole structure is still stable and can sustain the tensile load-bearing ability. Finally, in stage III, when the size of the defects extends to the critical value, brittle failure will occur in the whole structure, resulting in a slump of the potential energy. The interactions among A, D and R types in the neighboring cells are shown in figure S3. When uniaxial tension is applied on the monolayer GO, the epoxy-to-ether transformation occurs in the A unit first because the epoxy covalent bond in A undergoes more strain. After that, the D unit begins to be damaged by tension, as shown in figure S3(b). As the strain increases, the crack initiates here, and then propagates further along the defects. Note that in the R unit, only the hydroxyl group is not damaged because the tensile strain energy was released by the failure of units A and D. Furthermore, the closed-ring defects will be formed when the tensile strain increases to the yield point.

The fracture toughness of the sheets is calculated as a function of the strain rate, plotted in figure S4, along with size. Interestingly, the fracture toughness slightly decreases when the loading rate exceeds  $10000 \text{ m s}^{-1}$ , that is, the plasticity of the GO sheets will disappear under the high strain rate. The epoxy-to-ether transition under high-strain-rate loading would happen instantly so that the crack propagates along the linear defect, which will lead to the brittle fracture. The same phenomenon occurs as the size of the sample decreases to the critical value, which is 10 nm or less. Here, the critical value refers to the size that can maintain the closed-ring defects, that is, the GO sheets that exceed critical dimensions will show plasticity.

#### The influence of the proportion of oxygen functional groups

Besides the influence of the oxygen content, the proportion of the different oxygen functional groups also plays an important role in the mechanical properties of GO. From the tensile results of GOs (figure 6), it can be found that nonlinear-to-linear elastic transition mainly depends on the proportion of the epoxy and hydroxyl groups. In general, it has been verified that there are also many oxygen functional groups on the surface affecting the deformation properties of GO [26, 64]. Hence the monolayer GO models ( $f = 0.15$ ) with randomly distributed (R-GO) epoxy and hydroxyl groups with different ratios  $\varphi$  (1:0, 4:1, and 1:1) were built for uniaxial tension tests. We found that the chirality-dependence on mechanics disappears due to the random distribution of oxygen functional groups. Stress-strain results of the uniaxial tension which were performed in the armchair direction are demonstrated

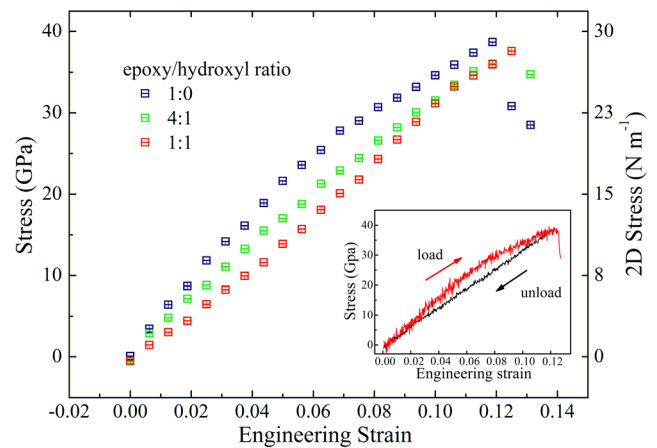


**Figure 6.** Mechanical properties of monolayer GO with randomly distributed oxygen functional groups ( $f = 0.15$ ,  $\varphi = 1:0$ ,  $4:1$ , and  $1:1$ ) under armchair tension. The red, green, and blue symbols denote different ratios of oxygen functional groups. The tensile strengths of different monolayer GOs in the armchair direction are calculated to be 37–39 GPa. A typical loading–unloading curve ( $\varphi = 1:1$ ) is illustrated in the bottom-right corner. The error bars correspond to  $\pm 1$  standard deviation in the material properties obtained from three different structures with random spatial distributions of functional groups.

in figure 6, where the red, green, and blue symbols denote the different ratios of the oxygen functional groups in R-GO. Interestingly, we found that all the strengths were approximately equivalent ( $\sigma_s = 37\text{--}39 \text{ GPa}$ ) in those three different cases, as well as the fracture strain ( $\sim 0.12$ ). This could be clarified by the fact that the quantity of  $sp^3$  carbon atoms changes slightly as the ratio  $\varphi$  increases to a certain range, and besides, the  $sp^2$  carbon network is disrupted by the local C–C  $sp^3$  hybridization of the functional groups, both of which determine the strength of monolayer GO [26]. However, there is an exception when  $\varphi$  is close to zero, in which the absence of epoxy groups results in thoroughly brittle fracture behaviors.

In particular, stress–strain curves in figure 6 reveal that the deformation processes of R-GOs exhibit a nonlinear–linear–nonlinear transition with an increasing hydroxyl ratio. Here, the first nonlinear elastic deformation refers to the strain-hardening behavior, that is, the modulus decreases as the strain increases. The linear elastic deformation means that the modulus of GO is a constant, whereas the second nonlinear elastic deformation is the strain-softening behavior, which is the reverse of the first case. A previous study considered that the nonlinear elastic deformation behaviors of pristine graphene, which is interpreted as strain-softening, could be simplified as the superposition effect of bond-stretching and angle-changing [65]. From this point of view, the nonlinear elastic behaviors of GO (i.e. red triangles in figure 6) can be explained by the strain-softening mechanism, that is hydroxyl groups cannot change the deformation mechanism when compared with graphene [66], merely reducing the stiffness by disturbing the  $sp^2$  bonds network. Moreover, a certain number of hydroxyl groups create significant hydrogen-bonding interaction, which is the reason why GOs with more hydroxyl groups possess a higher Young’s modulus. In addition, an unloading simulation was carried out in the case of  $\varphi = 1:1$  to



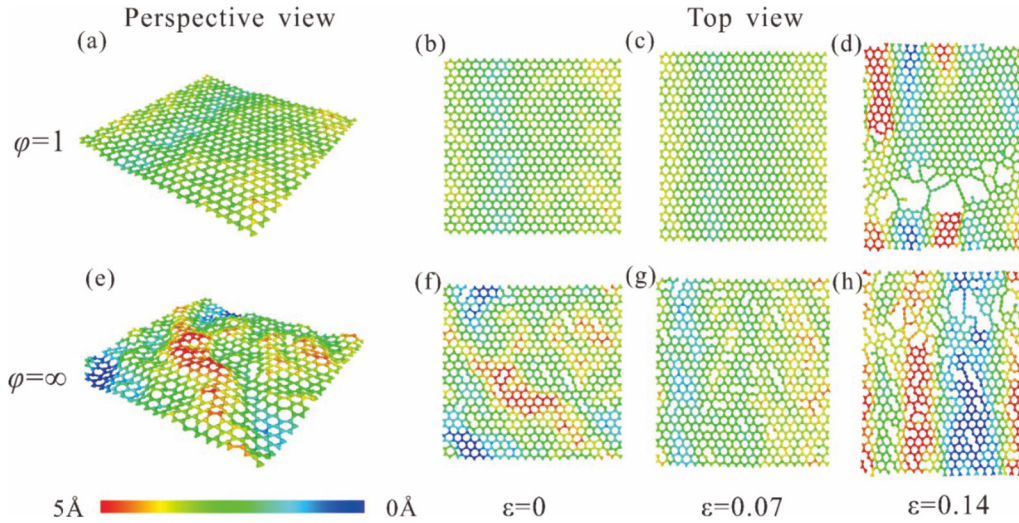


**Figure 7.** The colored height maps in the plane of GOs without displaying the functional groups.  $\varphi = 1$ : perspective view (a), top view (b)–(d);  $\varphi = \infty$ : perspective view (e), top view (f)–(h).

distinguish whether the GO is elastic or plastic before a fracture occurs. The stress–strain curve of this loading/unloading process is illustrated in the inset of figure 6, which indicates that the monolayer GO is elastic when the tensile strain is lower than 0.12 because there is no residual strain in the stress–strain curve. The increased ratio  $\varphi$  features the stress–strain result (green squares in figure 6) with linear elasticity. It means that the nonlinear elastic response could be suppressed by the epoxy groups, by which structure wrinkling of monolayer GO could be observed, resulting in the characteristic entropic elastic behaviors in a thin membrane structure, that is, the entropic elasticity is attributed to the wrinkling [35]. The entropic elasticity can also be interpreted as the strain-hardening mechanism. If both hydroxyl groups and epoxy groups are introduced into GO, the elastic deformation of GO will be determined by the strain-hardening or -softening competing mechanism. When the entropic contribution is balanced with the intrinsic nonlinear elasticity, the mechanical deformation of monolayer R-GO displays a linear elasticity, such as the result of  $\varphi = 4:1$  (figure 6). The results show that specific deformation characteristics can be readily achieved by changing the ratio of oxygen functional groups.

To further study the mechanism of wrinkle-induced entropic elasticity, we present the influence of epoxy groups and hydroxyl groups on the out-of-plane displacement of monolayer R-GO. Colored height maps during the tensile process are shown in figure 7. In the tensile direction, monolayer R-GO exhibits a distinct altitudinal difference (figure 7(e)), which means that the entropic elasticity induced by epoxy groups plays a greater role in the mechanical responses corresponding to the blue square symbols in figure 7(a) ( $\varphi = 1:0$ ). It is noted that the surface morphology of monolayer R-GO maintains wrinkling even during the whole tensile process, which is caused by vacancy and distorted defects evolving from the epoxy-to-ether transformation (figures 7(f) and (g)). Then monolayer GO will be flattened with a gradual increase in tensile strain, in which the tensile resistance keeps increasing because of the reduced degree of freedom. In addition, we find

that the two models both have significant height differences in the out-of-plane direction at 0.14 strain (figures 7(d) and (h)). This phenomenon can be referred to as lateral wrinkling, which mostly occurs in the thin membrane structure [28, 67], and the closed-ring defects (figures 7(d) and (h)) further confirm that monolayer GO with a certain proportion of epoxy groups is plastic when the tensile strain is beyond 0.12.

To gain further insight into this idiosyncratic elastic deformation, the continuum mechanics method has been utilized to understand the constitutive relation of graphene in a previous study [66]. The experimental force–deformation relation formula describes a nonlinear stress–strain relation as follows [4]:

$$\Sigma = E\eta + D\eta^2, \quad (3)$$

where  $E$  and  $D$  are the Young's modulus and the third-order nonlinear elastic modulus of monolayer graphene, respectively.  $\Sigma$  represents the second Piola–Kirchhoff stress and  $\eta$  is the Lagrangian strain. However, for the graphene with oxygen functional groups, the entropic elastic effect should be considered. Here, we propose an amendatory stress–strain formula:

$$\Sigma = (E - K_1\phi)\eta + (D + K_2\phi)\eta^2, \quad (4)$$

where  $K_1$ ,  $K_2$  are correction coefficients which could be related to the oxygen content, the atomistic distributions, and the ambient temperature, etc, and  $\phi$  is the relative content of the epoxy groups ( $\phi = N_{\text{epoxy}}/(N_{\text{epoxy}} + N_{\text{hydroxyl}})$ ). Here, the products of  $\phi$  and  $K_1$ , and  $K_2$  are a phenomenological description of the strain-hardening and -softening competing mechanism. Due to the complexity of the synergistic effect of such factors, we obtain the theoretical value of the coefficients by fitting the results ( $\phi = 0, 1$ ) computed in MD simulations. To demonstrate this modified formula, theoretical fitted stress–strain curves are demonstrated in figure 8 based on equation (2), in good agreement with MD simulated results ( $\phi = 0.5, 0.8$ ). In addition, the ultimate strength, ultimate strain, scalar nonlinear coefficients, and fitting parameters are listed in table 1, as compared with quantum chemical



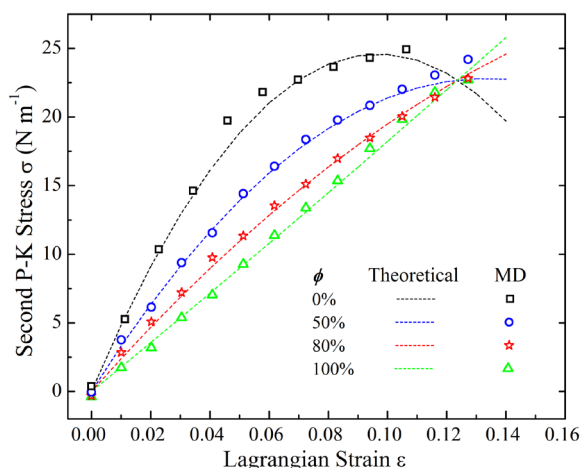


**Figure 8.** Comparison of theoretical stress–strain curves (lines) as defined in equation (2) with that from MD calculations (symbols).

**Table 1.** Ultimate strengths ( $\Sigma_u$ ), ultimate strains ( $\eta_u$ ) and the scalar nonlinear coefficients ( $E$ ,  $D$ ,  $K_1$ ,  $K_2$ ) of GO under uniaxial tension along the armchair direction, as compared with those of GO and graphene. The thickness of monolayer GO is assumed to be 0.7 nm, while that of graphene is assumed to be 0.34 nm.

	Graphene oxide ( $f = 0.15$ , $\varphi = 0-1$ )	Graphene oxide <sup>a</sup> ( $f = 0.5$ , $\varphi = 0.25-0.5$ )	Graphene <sup>b</sup>
$\Sigma_u$ ( $\text{N m}^{-1}$ )	25–31	~19	~34
$\eta_u$	0.12–0.14	~0.1	~0.2
$E$ ( $\text{N m}^{-1}$ )	508	270	310
$K_1$ ( $\text{N m}^{-1}$ )	–331	–134	...
$D$ ( $\text{N m}^{-1}$ )	–2623	...	–1050
$K_2$ ( $\text{N m}^{-1}$ )	2675	...	...

<sup>a</sup>First-principles computation [26].

<sup>b</sup>Tight-binding atomistic simulation [67].

calculations. This theoretical stress–strain formula may be useful for the study of the complicated deformation of GO or other graphene derivatives. It should be noted that equation (4) is a semi-empirical formula of the description of nonlinear elastic behavior, which is only valid within the elastic deformation stage. Thus, when it reaches the fracture stage, the semi-empirical formula equation (4) will fail. Based on the constitutive relation of graphene, we calculated the elastic modulus and the third order modulus of ten models by fitting the stress–strain relation. There are strong linear relationships between the modulus and oxygen content. Thus, the results of the linear fitting are used in place of terms  $E$  and  $D$  to define the deformation behavior of the GO. The correction factors ( $K_1$  and  $K_2$ ) mainly represent the influence of the oxygen content on the modulus, that is, the modification is valid only for the elastic deformation stage.

## Conclusions

In conclusion, by changing the content, distribution and proportion of oxygen functional groups, some anomalous in-plane mechanical properties of GO monolayer are

systematically investigated. The monolayer GO exhibits a brittle–ductile–brittle transition as the oxygen content increases from 0.05–0.45, which is mainly due to the different defect evolution mechanisms. We find that the arm-chair-arranged epoxy groups cause the chirality-dependent plasticity, resulting from the epoxy-to-ether transformation-induced closed-ring defects. For diagonal-patterned epoxy groups, diagonal symmetric defects can weaken such chirality-dependent plasticity. These analyses further explain the plastic fracture behavior of GO. On the other hand, when changing the proportion of oxygen functional groups, GO exhibits the strain-hardening or -softening competing mechanism which dominates the linear–nonlinear–linear elastic deformation. After combining the influences of in-plane and out-of-plane characteristics, such as covalent bonds, hydroxyl bonds interaction and entropic elasticity, we further propose a modified stress–strain formula to illustrate the deformation mechanism based on the continuum mechanics theory, which agrees well with the MD results. These results demonstrate that the elastic–plastic mechanical properties of graphene can be engineered through the oxygen functional groups, which can be extended to other 2D materials.

## Acknowledgments

This work was jointly supported by the Strategic Priority Research Program of the Chinese Academy of Sciences (XDB22040402), the Science Challenge Project (TZ2016001), and the National Natural Science Foundation of China (11525211). The numerical calculations have been conducted on the supercomputing system in the Supercomputing Center of University of Science and Technology of China.

## ORCID iDs

YinBo Zhu  <https://orcid.org/0000-0001-9204-9300>

## References

- [1] Hu S *et al* 2014 Proton transport through one-atom-thick crystals *Nature* **516** 227–30
- [2] Novoselov K S, Fal V, Colombo L, Gellert P, Schwab M and Kim K 2012 A roadmap for graphene *Nature* **490** 192–200
- [3] Geim A K 2009 Graphene: status and prospects *Science* **324** 1530–4
- [4] Lee C, Wei X, Kysar J W and Hone J 2008 Measurement of the elastic properties and intrinsic strength of monolayer graphene *Science* **321** 385–8
- [5] Geim A K and Novoselov K S 2007 The rise of graphene *Nat. Mater.* **6** 183–91
- [6] Ramanathan T, Abdala A, Stankovich S, Dikin D, Herrera-Alonso M, Piner R, Adamson D, Schniepp H, Chen X and Ruoff R 2008 Functionalized graphene sheets for polymer nanocomposites *Nat. Nanotechnol.* **3** 327–31
- [7] Stankovich S, Dikin D A, Dommett G H, Kohlhaas K M, Zimney E J, Stach E A, Piner R D, Nguyen S T and Ruoff R S 2006 Graphene-based composite materials *Nature* **442** 282–6

- [8] Lee H, Choi T K, Lee Y B, Cho H R, Ghaffari R, Wang L, Choi H J, Chung T D, Lu N and Hyeon T 2016 A graphene-based electrochemical device with thermoresponsive microneedles for diabetes monitoring and therapy *Nat. Nanotechnol.* **11** 566–72
- [9] Zhu Y, Wang F, Bai J, Zeng X C and Wu H 2015 Compression limit of two-dimensional water constrained in graphene nanocapillaries *ACS Nano* **9** 12197–204
- [10] Rogers G W and Liu J Z 2011 High-performance graphene oxide electromechanical actuators *J. Am. Chem. Soc.* **134** 1250–5
- [11] Dai Z, Liu L, Qi X, Kuang J, Wei Y, Zhu H and Zhang Z 2016 Three-dimensional sponges with super mechanical stability: harnessing true elasticity of individual carbon nanotubes in macroscopic architectures *Sci. Rep.* **6** 18930
- [12] Wu Y, Yi N, Huang L, Zhang T, Fang S, Chang H, Li N, Oh J, Lee J A and Kozlov M 2015 Three-dimensionally bonded spongy graphene material with super compressive elasticity and near-zero Poisson's ratio *Nat. Commun.* **6** 6141
- [13] Kuang J, Dai Z, Liu L, Yang Z, Jin M and Zhang Z 2015 Synergistic effects from graphene and carbon nanotubes endow ordered hierarchical structure foams with a combination of compressibility, super-elasticity and stability and potential application as pressure sensors *Nanoscale* **7** 9252–60
- [14] Liu L, Gao Y, Liu Q, Kuang J, Zhou D, Ju S, Han B and Zhang Z 2013 High mechanical performance of layered graphene oxide/poly (vinyl alcohol) nanocomposite films *Small* **9** 2466–72
- [15] Compton O C, Cranford S W, Putz K W, An Z, Brinson L C, Buehler M J and Nguyen S T 2012 Tuning the mechanical properties of graphene oxide paper and its associated polymer nanocomposites by controlling cooperative intersheet hydrogen bonding *ACS Nano* **6** 2008–19
- [16] Gao Y, Liu L-Q, Zu S-Z, Peng K, Zhou D, Han B-H and Zhang Z 2011 The effect of interlayer adhesion on the mechanical behaviors of macroscopic graphene oxide papers *ACS Nano* **5** 2134–41
- [17] Jiang Z, Xia D, Li Y, Li J, Li Q, Chen M, Huang Y, Besenbacher F and Dong M 2013 Facilitating the mechanical properties of a high-performance pH-sensitive membrane by cross-linking graphene oxide and polyacrylic acid *Nanotechnology* **24** 335704
- [18] Park S and Ruoff R S 2009 Chemical methods for the production of graphenes *Nat. Nanotechnol.* **4** 217–24
- [19] Amadei C A, Stein I Y, Silverberg G J, Wardle B L and Vecitis C D 2016 Fabrication and morphology tuning of graphene oxide nanoscrolls *Nanoscale* **8** 6 783–91
- [20] Joshi R K, Carbone P, Wang F C, Kravets V G, Su Y, Grigorieva I V, Wu H A, Geim A K and Nair R R 2014 Precise and ultrafast molecular sieving through graphene oxide membranes *Science* **343** 752–4
- [21] Yan M et al 2013 Nanowire templated semihollow bicontinuous graphene scrolls: designed construction, mechanism, and enhanced energy storage performance *J. Am. Chem. Soc.* **135** 18176–82
- [22] Dikin D A, Stankovich S, Zimney E J, Piner R D, Dommett G H, Evmenenko G, Nguyen S T and Ruoff R S 2007 Preparation and characterization of graphene oxide paper *Nature* **448** 457–60
- [23] Liu Q, Liu L, Xie K, Meng Y, Wu H, Wang G, Dai Z, Wei Z and Zhang Z 2015 Synergistic effect of ar-GO/PANI nanocomposite electrode based air working ionic actuator with a large actuation stroke and long-term durability *J. Mater. Chem. A* **3** 8380–8
- [24] Jo G, Choe M, Lee S, Park W, Kahng Y H and Lee T 2012 The application of graphene as electrodes in electrical and optical devices *Nanotechnology* **23** 112001
- [25] Zheng Q B, Geng Y, Wang S J, Li Z G and Kim J K 2010 Effects of functional groups on the mechanical and wrinkling properties of graphene sheets *Carbon* **48** 4315–22
- [26] Liu L, Zhang J, Zhao J and Liu F 2012 Mechanical properties of graphene oxides *Nanoscale* **4** 5910–6
- [27] Wang C et al 2014 Mechanical characteristics of individual multi-layer graphene-oxide sheets under direct tensile loading *Carbon* **80** 279–89
- [28] Polyzos I, Bianchi M, Rizzi L, Koukaras E N, Parthenios J, Papagelis K, Sordan R and Galiotis C 2015 Suspended monolayer graphene under true uniaxial deformation *Nanoscale* **7** 13033–42
- [29] Cao C H, Daly M, Singh C V, Sun Y and Filleter T 2015 High strength measurement of monolayer graphene oxide *Carbon* **81** 497–504
- [30] Suk J W, Piner R D, An J and Ruoff R S 2010 Mechanical properties of monolayer graphene oxide *ACS Nano* **4** 6557–64
- [31] Kang S-H, Fang T-H, Hong Z-H and Chuang C-H 2013 Mechanical properties of free-standing graphene oxide *Diam. Relat. Mater.* **38** 73–8
- [32] López-Polín G, Gómez-Navarro C, Parente V, Guinea F, Katsnelson M I, Pérez-Murano F and Gómez-Herrero J 2015 Increasing the elastic modulus of graphene by controlled defect creation *Nat. Phys.* **11** 26–31
- [33] López-Polín G, Gómez-Herrero J and Gómez-Navarro C 2015 Confining crack propagation in defective graphene *Nano Lett.* **15** 2050–4
- [34] Zandiashbar A, Lee G-H, An S J, Lee S, Mathew N, Terrones M, Hayashi T, Picu C R, Hone J and Koratkar N 2014 Effect of defects on the intrinsic strength and stiffness of graphene *Nat. Commun.* **5** 3186
- [35] Zhang T, Li X, Kadkhodaei S and Gao H 2012 Flaw insensitive fracture in nanocrystalline graphene *Nano Lett.* **12** 4605–10
- [36] Xu L, Wei N and Zheng Y 2013 Mechanical properties of highly defective graphene: from brittle rupture to ductile fracture *Nanotechnology* **24** 505703
- [37] Wei X D, Mao L, Soler-Crespo R A, Paci J T, Huang J X, Nguyen S T and Espinosa H D 2015 Plasticity and ductility in graphene oxide through a mechanochemically induced damage tolerance mechanism *Nat. Commun.* **6** 8029
- [38] Plimpton S 1995 Fast parallel algorithms for short-range molecular dynamics *J. Comput. Phys.* **117** 1–19
- [39] Fonseca A F, Liang T, Zhang D F, Choudhary K and Sinnott S B 2016 Probing the accuracy of reactive and non-reactive force fields to describe physical and chemical properties of graphene-oxide *Comput. Mater. Sci.* **114** 236–43
- [40] Cao C H, Daly M, Chen B, Howe J Y, Singh C V, Filleter T and Sun Y 2015 Strengthening in graphene oxide nanosheets: bridging the gap between interplanar and intraplanar fracture *Nano Lett.* **15** 6528–34
- [41] Chen N, Lusk M T, van Duin A C and Goddard W A III 2005 Mechanical properties of connected carbon nanorings via molecular dynamics simulation *Phys. Rev. B* **72** 085416
- [42] Van Duin A C, Dasgupta S, Lorant F and Goddard W A 2001 ReaxFF: a reactive force field for hydrocarbons *J. Phys. Chem. A* **105** 9396–409
- [43] Liu X Y, Wang F C, Park H S and Wu H A 2013 Defecting controllability of bombarding graphene with different energetic atoms via reactive force field model *J. Appl. Phys.* **114** 054313
- [44] Xia J, Liu X, Zhou W, Wang F and Wu H 2016 Transformation between divacancy defects induced by an energy pulse in graphene *Nanotechnology* **27** 274004
- [45] Chenoweth K, Van Duin A C T and Goddard W A. 2008 ReaxFF reactive force field for molecular dynamics

- simulations of hydrocarbon oxidation *J. Phys. Chem. A* **112** 1040–53
- [46] Berendsen H J, Postma J V, van Gunsteren W F, DiNola A and Haak J 1984 Molecular dynamics with coupling to an external bath *J. Chem. Phys.* **81** 3684–90
- [47] Tsai D 1979 The virial theorem and stress calculation in molecular dynamics *J. Chem. Phys.* **70** 1375–82
- [48] Subramaniyan A K and Sun C T 2008 Continuum interpretation of virial stress in molecular simulations *Int. J. Solids Struct.* **45** 4340–6
- [49] Peng Q, Ji W and De S 2012 Mechanical properties of the hexagonal boron nitride monolayer: *ab initio* study *Comput. Mater. Sci.* **56** 11–7
- [50] Mattevi C, Eda G, Agnoli S, Miller S, Mkhoyan K A, Celik O, Mastrogiovanni D, Granozzi G, Garfunkel E and Chhowalla M 2009 Evolution of electrical, chemical, and structural properties of transparent and conducting chemically derived graphene thin films *Adv. Funct. Mater.* **19** 2577–83
- [51] Li X, Zhang G, Bai X, Sun X, Wang X, Wang E and Dai H 2008 Highly conducting graphene sheets and Langmuir–Blodgett films *Nat. Nano* **3** 538–42
- [52] Lerf A, He H, Forster M and Klinowski J 1998 Structure of graphite oxide revisited *J. Phys. Chem. B* **102** 4477–82
- [53] Peng Q and De S 2013 Mechanical properties and instabilities of ordered graphene oxide C 6 O monolayers *RSC Adv.* **3** 24337–44
- [54] Gao W, Alemany L B, Ci L and Ajayan P M 2009 New insights into the structure and reduction of graphite oxide *Nat. Chem.* **1** 403–8
- [55] Stankovich S, Dikin D A, Piner R D, Kohlhaas K A, Kleinhammes A, Jia Y, Wu Y, Nguyen S T and Ruoff R S 2007 Synthesis of graphene-based nanosheets via chemical reduction of exfoliated graphite oxide *Carbon* **45** 1558–65
- [56] Yan J-A and Chou M Y 2010 Oxidation functional groups on graphene: structural and electronic properties *Phys. Rev. B* **82** 125403
- [57] Wang L, Sun Y Y, Lee K, West D, Chen Z F, Zhao J J and Zhang S B 2010 Stability of graphene oxide phases from first-principles calculations *Phys. Rev. B* **82** 161406
- [58] Yan J-A, Xian L and Chou M Y 2009 Structural and electronic properties of oxidized graphene *Phys. Rev. Lett.* **103** 086802
- [59] Krishnamoorthy K, Veerapandian M, Yun K and Kim S J 2013 The chemical and structural analysis of graphene oxide with different degrees of oxidation *Carbon* **53** 38–49
- [60] Yang D et al 2009 Chemical analysis of graphene oxide films after heat and chemical treatments by x-ray photoelectron and Micro-Raman spectroscopy *Carbon* **47** 145–52
- [61] Zhao H, Min K and Aluru N 2009 Size and chirality dependent elastic properties of graphene nanoribbons under uniaxial tension *Nano Lett.* **9** 3012–5
- [62] Zhang P et al 2014 Fracture toughness of graphene *Nat. Commun.* **5** 3782
- [63] Kosynkin D V, Higginbotham A L, Sinitskii A, Lomeda J R, Dimiev A, Price B K and Tour J M 2009 Longitudinal unzipping of carbon nanotubes to form graphene nanoribbons *Nature* **458** 872–6
- [64] Liu L, Wang L, Gao J, Zhao J, Gao X and Chen Z 2012 Amorphous structural models for graphene oxides *Carbon* **50** 1690–8
- [65] Zhou L and Cao G 2016 Nonlinear anisotropic deformation behavior of a graphene monolayer under uniaxial tension *Phys. Chem. Chem. Phys.* **18** 1657–64
- [66] Cadelano E, Palla P L, Giordano S and Colombo L 2009 Nonlinear elasticity of monolayer graphene *Phys. Rev. Lett.* **102** 235502
- [67] Cerda E and Mahadevan L 2003 Geometry and physics of wrinkling *Phys. Rev. Lett.* **90** 074302